Mechanics of Materials 164 (2022) 104113

Contents lists available at ScienceDirect

Mechanics of Materials

journal homepage: www.elsevier.com/locate/mechmat

Failure sequence determination in sandwich structures using concurrent acoustic emission monitoring and postmortem thermography

Isa Emami Tabrizi [a,b,c], Fatih Ertugrul Oz [b,d], Jamal Seyyed Monfared Zanjani [e], Sefa Kemal Mandal [a,b,c], Mehmet Yildiz [a,b,c,*]

[a] Integrated Manufacturing Technologies Research and Application Center, Sabanci University, Tuzla, 34956, Istanbul, Turkey
[b] Composite Technologies Center of Excellence, Sabanci University-Kordsa, Istanbul Technology Development Zone, Sanayi Mah. Teknopark Blvd. No: 1/1B, Pendik, 34906, Istanbul, Turkey
[c] Faculty of Engineering and Natural Sciences, Sabanci University, Tuzla, 34956, Istanbul, Turkey
[d] Department of Mechanical Engineering, Istanbul Gedik University, Kartal, 34876, Istanbul, Turkey
[e] Faculty of Engineering Technology, University of Twente, 7500AE, Enschede, the Netherlands

ARTICLE INFO

Keywords:
Sandwich panel composites
Acoustic emission
Thermography
Damage analysis
Flexural strength

ABSTRACT

This study provides a novel approach for damage classification and failure sequence evaluation in sandwich panel composite materials under flexural loading condition merely by using acoustic emission monitoring in interrupted mechanical tests and postmortem lock in thermography analysis. The studied sandwich panels consist of glass fiber reinforced phenolic skins and Nomex honeycomb core which are used extensively in the aerospace industry. While one of the standard flexural samples is mechanically tested up to global failure, the other specimens are loaded till a certain load level and the tests are interrupted. Acoustic emission hits are recorded throughout the mechanical tests by using piezoelectric sensors, and are classified using a well-established clustering algorithm. The damaged samples are then investigated via lock in thermography technique to identify the hidden failure progress inside the sandwich structure. Acoustic emission monitoring is successfully used to mark the change of mechanical response under flexural loading condition. The results of acoustic emission analysis indicated four different clusters associated with four major failure modes occurring due to mechanical loading. Correlating failure progress observed in thermography results with the fraction of acoustic emission clusters registered during mechanical tests helped to attribute each class of acoustic emission hits to a specific failure type. Upon using the interrupted test methodology together with the lock-in thermography technique, one can reliably identify the damage types and their sequence of manifestation during flexural tests. The results show that successful analysis of visually hidden failure progress in sandwich panel composites under out of plane loading condition can be attained by using structural health monitoring techniques and quasi static tests.

1. Introduction

Sandwich panels composites (SPCs) consisting of thin but rigid facesheets and thick lightweight core are developed for achieving superior out of plane strength at remarkable low weight. Such panels have found a place in many application in areas such as aerospace, marine and civil structures where weight reduction and mechanical reliability are essential. Despite their advantages, SPCs are prone to stiffness degradation and out of plane strength reduction due to the initiation and growth of damages including fiber breakage in facesheets, core/facesheet debonding and core crush (Olsson, 1998). These root causes of these might be associated with the individual or concurrent presence of factors such as manufacturing defects, unexpected loads, and environmental factors. Hence, understanding the initiation and evolution of damage inside sandwich panels is an important step to optimize their design and prevent possible failures (Sikdar et al., 2018).

Due to key importance of out of plane strength in SPCs, investigation regarding damage growth in these composite materials under flexural loading condition has been carried out in numerous studies. These efforts discuss the effect of material, facesheet/core bonding, geometry and loading rate on out of plane response of sandwich structures and consequent stiffness reduction stages. Some of the relevant studies are

* Corresponding author. Integrated Manufacturing Technologies Research and Application Center, Sabanci University, Tuzla, 34956 Istanbul, Turkey.
E-mail address: mehmet.yildiz@sabanciuniv.edu (M. Yildiz).

https://doi.org/10.1016/j.mechmat.2021.104113
Received 20 May 2021; Received in revised form 3 October 2021; Accepted 14 October 2021
Available online 16 October 2021

summarized as follows. Li et al. (Li and Ma, 2020), divided ductile flexural response of basalt fiber resin-based sheets and Nomex honeycomb sandwich panels into five stages namely, initial elastic region, yielding, stacking (complete crush of core material), sheet bending and sheet breakage. Shi et al. (2014), investigated the effect of short Kevlar-fiber interfacial toughening at the interface between the carbon-fiber facesheets and aluminum-honeycomb core under flexural loading. Their results revealed that interfacial toughening prevented interface debonding and promoted facesheet breakage at peak load. Zaharia et al. (2017), confirmed that higher quality of the bonding between CFRP facesheets and Nomex honeycomb core prevented interfacial delamination under various loading conditions. In another study, Topkaya et al. (Topkaya and Solmaz, 2016), showed that thickness increment of honeycomb core increased the fatigue life of sandwich composites under cyclic bending loads. Liu et al. (2019), exhibited that Nomex honeycomb with high shear strength could increase the effect of thick facesheets and improve the overall strength of sandwich composite. Giglio et al. (2012), classified the degradation modes of sandwich panels with aluminum skins and Nomex honeycomb core under flexural loading into face yielding, face wrinkling, intra-cell dimpling, core shear and local indentation. Anandan et al. (2020), used experimental approach and a numerical model to show that high temperatures decreased the load bearing capacity of sandwich panel while having small effect on stiffness. Finally Medina et al. (2020), have mentioned that manufacturing defects can harden the prediction of damage progress under flexural loading for sandwich composites. Despite all these efforts, proper scrutinization of damage mechanisms in sandwich panels can only be achieved via real time monitoring methods.

Using structural health monitoring techniques such as digital image correlation (Tabrizi et al., 2021), thermography (AlKhateab et al., 2020; Khan et al., 2020), fiber Bragg gratings (Yilmaz et al., 2016; Akay et al., 2016; Kocaman et al., 2017; Kefal et al., 2021), acoustic emission (AE) (Yilmaz and Yildiz, 2017; Oz et al., 2017, 2018) and guided waves method (Yilmaz et al., 2020; Seno et al., 2019) have proven to be efficient tools for understanding the damage mechanism and shape sensing in composite materials (Kefal et al., 2021). However, the necessity of real time fulfillment of four stages of structural health monitoring approach namely, damage initiation detection, damage classification, damage severity assessment and damage localization are best satisfied by using acoustic emission analysis (Saeedifar et al., 2021).

Damage initiation and accumulation inside materials is accompanied by emission of elastic waves which can be detected using surface mounted piezoelectric sensors. Each propagating acoustic wave inside the material has its specific descriptors associated with the wave source and failure characteristics. Time and frequency domain features of waves such as energy, counts, rise time and amplitude can be utilized to analyze damage evolution under various loading conditions (Tabrizi et al., 2019). Accordingly, investigators have correlated damage growth rate in composite materials with observed trends in AE results (He et al., 2021). Recent studies provide a comprehensive overview about damage characterization in composite materials via AE analysis (Barile et al., 2020; Saeedifar and Zarouchas, 2020). Several studies in literature have focused on the usage of AE to localize damages in sandwich panels (Leone et al., 2008; Masmoudi et al., 2015; Wu et al., 2021; Sikdar et al., 2019; Dikshit et al., 2021; Ciampa and Meo, 2010) while other investigators have used in-situ damage AE monitoring under various loading conditions to understand failure progress in sandwich panels (Masmoudi et al., 2015; Lee et al., 2009; Quispitupa et al., 2004; McGugan et al., 2006; Ben Ammar et al., 2014; Selmi et al., 2020; Uzal et al., 2018; Lainé et al., 2020; Essassi et al., 2020; Beylergil et al., 2020a; Harizi et al., 2021).

Selmi et al. (2020), clustered AE hits by using k-means algorithm under compression loading condition for a novel honeycomb core made of short flax fibers reinforced epoxy. Their results revealed that matrix failure was the dominant failure mode and an increase in fiber content of honeycomb structure could promote abrupt failure in the system. Uzal et al. (2018), investigated the flexural behavior of novel sandwich panel material in which both egg-crate shaped core and facesheets were made of E-glass fiber reinforced resin. Detailed analysis based on AE energy and cumulative AE counts successfully indicated the first ply failure moment under flexural loading condition. In another work, investigators studied damage mechanisms under internal pressure for two types of bottle shaped sandwich structures by using average frequency and RA values of AE hits (Lainé et al., 2020). They have signified that the damping capacity of sandwich structure could make damage monitoring through AE very challenging. Essassi et al., studied the bending behaviour of 3D-printed bio-based sandwich structures composites under fatigue cycles by monitoring the peak amplitude values of AE hits (Essassi et al., 2020). Low amplitude and high amplitude AE events were correlated with initiation of damage at skin, and propagation in core and skin/core debonding respectively. Harizi et al. (2021), used AE amplitude and cumulative absolute AE energy to monitor damage growth under flexural loading of carbon-reinforced thermoplastic sandwich composites. They have divided AE data into three clusters namely, matrix cracking, delamination and fiber rupture in the order of amplitude increment. Recently authors investigated usage of AE to determine failure types in glass fiber reinforced composite/metal sandwich structures interleaved with nonwoven thermoplastic layers (Beylergil et al., 2020b). They applied k-means clustering algorithm to distinguish various failure types and show that specific AE events correlated with debonding would decrease due to interface modification.

In addition to AE, several studies have indicated advantages of using active thermography as a non-destructive method to characterize damages in SPCs (Toscano et al., 2014; Zhao et al., 2017). Meola et al., used lock in thermography to reveal the locations of thick adhesive layer, cell edge cutting, frayed edge cells and absence of adhesive in carbon fiber reinforced polymer skins/Nomex core sandwich panels (Meola et al., 2006). Taraghi et al., used to thermography to reveal the effect of adding multi-walled carbon nanotubes in reduction of facesheet/core debonding due to impact loading in sandwich laminates (Taraghi and Fereidoon, 2016). Shrestha et al., used various image processing algorithms to post-process lock in thermography results and detect water ingress region inside honeycomb sandwich panels (Shrestha et al., 2019). They have concluded that the best data analysis algorithm for damage detection can be chosen via quantification of signal to noise ratio at damage location. Zhao et al., used lock in thermography to investigate debonding between titanium alloy skin/honeycomb panels (Zhao et al., 2017). Recently, Moghaddam et al., used thermography to quantify impact damage area in sandwich panels with hybrid facesheets and embedded shape memory alloy wires (MasoudiMoghaddam et al., 2020). All these methods have investigated damages and/or artificial defects in sandwich panels after mechanical loading or under no load condition. There are no studies to investigate damage growth inside SPCs via interrupted thermography inspection.

To the extent of authors' knowledge, no comprehensive investigation has been conducted to scrutinize failure progress in sandwich panels consisting glass fiber reinforced phenolic skin and Nomex® core. Moreover, stepwise study of flexural behavior of sandwich panels using AE analysis and lock-in thermography has not been reported yet. Although numerous studies have presented visual monitoring of samples as a method to define failure stages for sandwich structures, no specific study has used an interrupted test approach accompanied by structural health monitoring techniques to determine damage sequence in these materials. Moreover, the acoustic emission based damage identification relying on visual inspection is limited to visually discernible damages through the thickness of the sandwich panel. Considering the evermore utilization of these types of sandwich panels in aerospace and civil structures, and incapability of visual inspection to determine the internal failure progress in sandwich structures, a detailed and systematic study for their damage mechanisms is deemed. Therefore, this study aims to fill these gaps and provide an efficient approach for damage growth analysis in sandwich panels where the failure progress is

monitored and followed by a detailed postmortem analysis. Experimental approach used in this investigation utilizes correlation between AE, active thermography and microscopy to provide reliable evidence of failure stages of a sandwich panel used in aerospace structures. In other words, the results of this study not only are expected to validate other studies in the field, but they will offer new data for failure mechanisms in sandwich panels.

The subsequent sections of the manuscript are given as follows. In the first part, materials and manufacturing technique as well as experimental procedure used for flexural tests is explained thoroughly. The aspects of interrupted bending tests accompanied by AE monitoring and subsequent details of lock-thermography are explained. The next section describes the details of clustering AE data and their correlation with observed thermography images. Finally, the different stages of flexural behavior in tested sandwich panels are defined according to obtained results and concluding remarks are briefed.

2. Materials and experimental procedure

2.1. Sandwich panels

The studied composite material is a sandwich panel structure produced for aircraft interiors by Kordsa and is comprised of single layer glass fiber reinforced phenolic skins and Nomex® honeycomb cores. Surface plies have 8-harness-satin weave style with 300 gr/m^2 and 50% resin content. The core material had a height of 9.65 mm, a cell size of 3.2 mm and a density of 48 kg/m^3. The upper and lower skins and the Nomex honeycomb core of the specimens were stuck together using a non-woven 0.11 mm thick nylon adhesive film. The schematic of stacking sequence for sandwich panel is given in Fig. 1. The produced sandwich panels were cut into size of 250 mm × 75 mm according to the geometrical requirement of ASTM C393 test standard (International, 2020). Since honeycomb cores show higher strength in W direction (perpendicular to ribbon edges) as compared to L-direction, this anisotropy of strength is used as a design parameter for the design of interior parts in aviation industry. Hence, the length of samples in this study was aligned with W-direction of the honeycomb core.

2.2. Flexural tests and acoustic emission monitoring

In order to investigate the mechanical behavior of the honeycomb core sandwich samples, 3-point bending tests were conducted according to procedure given in ASTM C393 (International, 2020) test standard as seen in Fig. 2 (a). A 3-point bending test can only provide failure strength and stiffness of a structure. It is not sufficient to determine damage evolution before final failure. Because of this, acoustic emission (AE) is preferred to detect damage initiation and progression under loading. AEwin PCI2-4 software and Mistras PCI 2 acoustic emission apparatus were used to register AE hits throughout the test. Two piezoelectric sensors named PICO from Physical acoustic were used and fixed linearly along the midline of the top surface of bending test specimens using hot glue adhesive as shown in the Fig. 2a. The used AE sensors had operating frequency range of 250–750 kHz and a resonant frequency of 550 kHz. Two 0/2/4 type preamplifiers were used to amplify the strength of the logged acoustic signals. The preamplifiers were set to 20 dB gain value and single mode input. Pencil lead break test was conducted to make sure that both attached sensors could obtain required sensitivity before the test. Data acquisition parameters based on AE hardware manual were set to 40 dB for threshold, 50 μs for peak definition time (PDT), 100 μs as hit definition time (HDT) and 300 μs for hit lock-out time (HLT). The sampling rate during data acquisition was 2 MHz for each sensor. Necessary features (i.e. Amplitude, Average frequency, Peak frequency, Counts, Rise time, etc.) were extracted from recorded hits in time and frequency domains simultaneously as the tests proceeded. Noesis 7 software was used to further post-process of the data using a Bessel band-pass filter between 20 kHz and 800 kHz.

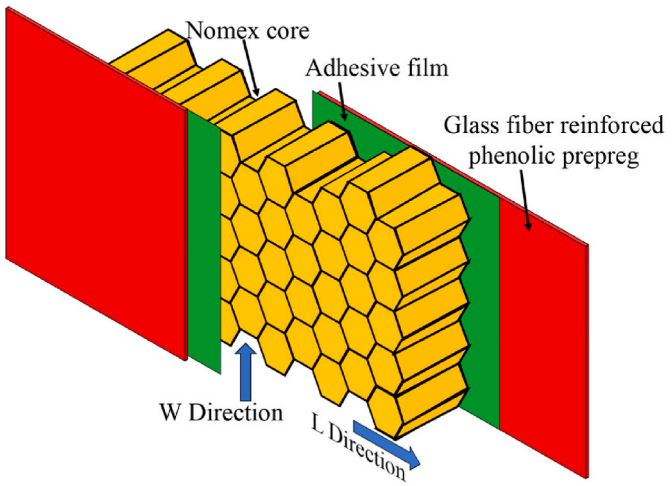

Fig. 1. Schematic of sandwich panel stacking sequence.

Mechanical tests were performed up to specific load levels, i.e. interrupted tests, to conduct the progressive damage monitoring as shown in Fig. 2b. The critical points of flexural behavior were characterized by conducting a complete bending test up to failure point of a sample henceforward known as Sp. 1. Then the evolution acoustic emission cumulative energy for Sp. 1 was recorded up to maximum failure load of 950 N and the load levels at which sudden upsurge of cumulative acoustic emission energy appeared were indicated as the critical load levels. These vital load levels were used as test end points for other samples. Accordingly, flexural tests for other samples namely, Sp. 2 and Sp. 3 were conducted up to 900 N and 920 N load levels, respectively. The registered AE data is clustered using the k-means++ pattern recognition algorithm to identify the damage types due to bending deformation in the sandwich laminates. The used algorithm has been successfully implemented previously at various investigations and its robustness for damage characterization in composite materials has been proven (Oz et al., 2017, 2018, 2019, 2020; Li et al., 2014, 2015). Even though the details of this algorithm has been given in referred papers, a concise information is provided for the sake of improving the self-consistency and readability of the current manuscript.

The used clustering scheme consists of 5 steps. First stage is transferring registered acoustic emission data for post processing in the algorithm. The second step comprises of choosing statistically representative and relevant acoustic emission features which possess highest Laplacian scores and minimum inter-correlation. Using these scoring schemes, the representative AE descriptors are ranked based on their statistical importance and the ones with the least correlation are distinguished. Third step of the utilized algorithm involves reduction of the multidimensional AE data into lower dimension sub-space with a new coordinate system comprised by Principal Component Analysis (PCA). At fourth step, the best possible number of clusters are chosen using two distinct evaluation indices namely, Silhouette coefficient and Davies-Bouldin index. Using these indices less dispersion of data with-in clusters and maximum possible partitioning of clusters is achieved. Finally, the k-means++ algorithm is implemented based on the chosen number of clusters at as presented in the complete flow chart of Fig. 3.

2.3. Lock-in thermography (LT) measurements

Even though AE can provide insight about damage progression, it cannot be reliable to interpret about the damage mode. An optical observation is required for a reliable identification. The performance of thermography was not tested previously for this aim. So, the interrupted flexural experiments were followed by lock-in thermography tests as seen in Fig. 4a to correlate and confirm the results of AE analysis with

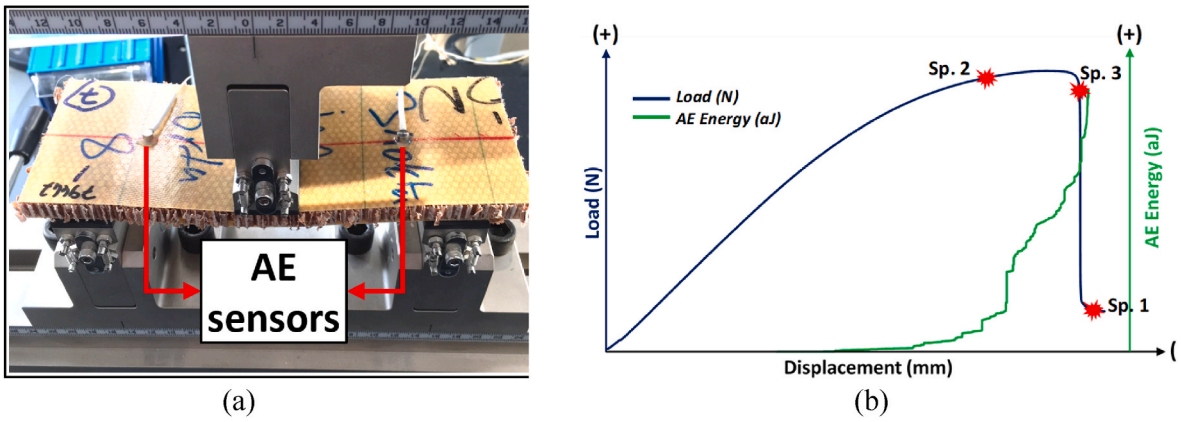

Fig. 2. a) Flexural test setup with attached AE sensors, b) Test interruption levels of specimens with respect to load vs. displacement diagram.

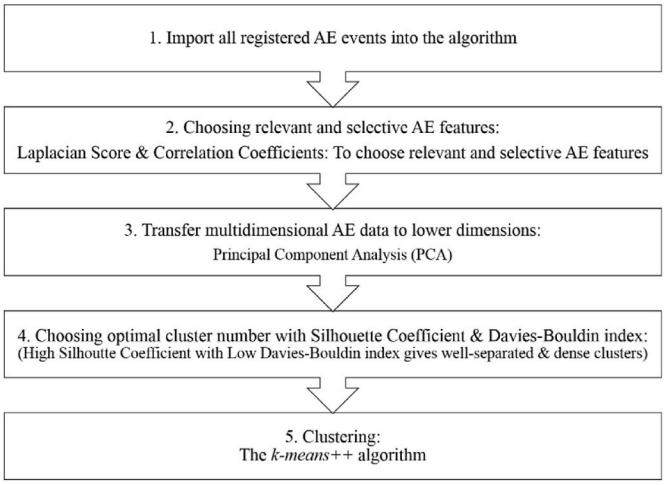

Fig. 3. Flowchart of k-means++ clustering algorithm.

thermography observations.

Xenon halogen lamps were used as heat source with the capability of producing modulated sinusoidal waveforms. FLIR X6580 thermal camera with 25 mm lens, Indium antimonide (InSb) photon detector and thermal sensitivity of 20 mK was used. The camera frame rate was set to 50 frames per second and the programmable generator named OTvis 6000 was used for stimulation of heat flux. Using Fast Fourier Transformation (FFT) capability of the Edevis DisplayImg 6 software, various informative images of the sample namely, phasegrams, temperature maps and real/imaginary parts of transformed photos were obtained. The thermal diffusion length, μ, inside a semi-infinite homogeneous material can be obtained from Fourier's law in one dimension as:

$$\mu = \sqrt{(2\alpha / \omega)} = \sqrt{(\alpha / \pi f)} \quad (1)$$

where ω is the modulation frequency, f is the wave frequency in Hz and α is the thermal diffusivity of the material. Effective thermal images that can present homogeneity status and the depth of defects (P) could be achieved at about double the thermal diffusion length as (Toscano et al., 2014):

$$P = 1.8 \times \mu \quad (2)$$

To ensure that thermal diffusivity is reasonable for inspection of anomalies through the thickness of the sandwich panels, lock in thermography was performed for one sample with a piece of black tape adhered to its rear side. The black tape exemplified debonded areas and inner failure at back surface of the samples on opposite side of the excitation lamps of lock in thermography procedure. The process of lock in thermography was performed at modulated frequencies of 1 Hz, 0.5 Hz, 0.1 Hz, 0.02 Hz, 0.01 Hz, and 0.002 Hz as seen in phasegrams of Fig. 4b. The results showed that the usage of lock in frequency equal to 0.002 Hz could clearly project the location and size of black tape with reasonable contrast to detect possible failure.

3. Results and discussion

3.1. Clustering of acoustic emission events

The results of the used algorithm in Fig. 5a-c show that the registered acoustic emission data is best represented with amplitude, peak frequency, weighted frequency and duration according to the Laplacian score and correlation coefficients. As seen in Fig. 5d, high Silhouette Coefficients and low Davies-Bouldin index meet at four and that is the

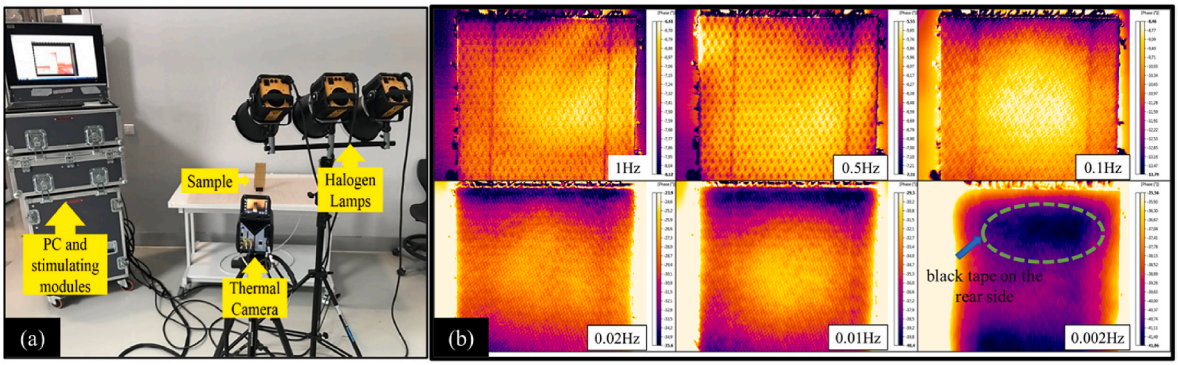

Fig. 4. a) Test set up for lock in thermography; b) Lock in thermography phasegram results to find the appropriate modulated frequency for inspection.

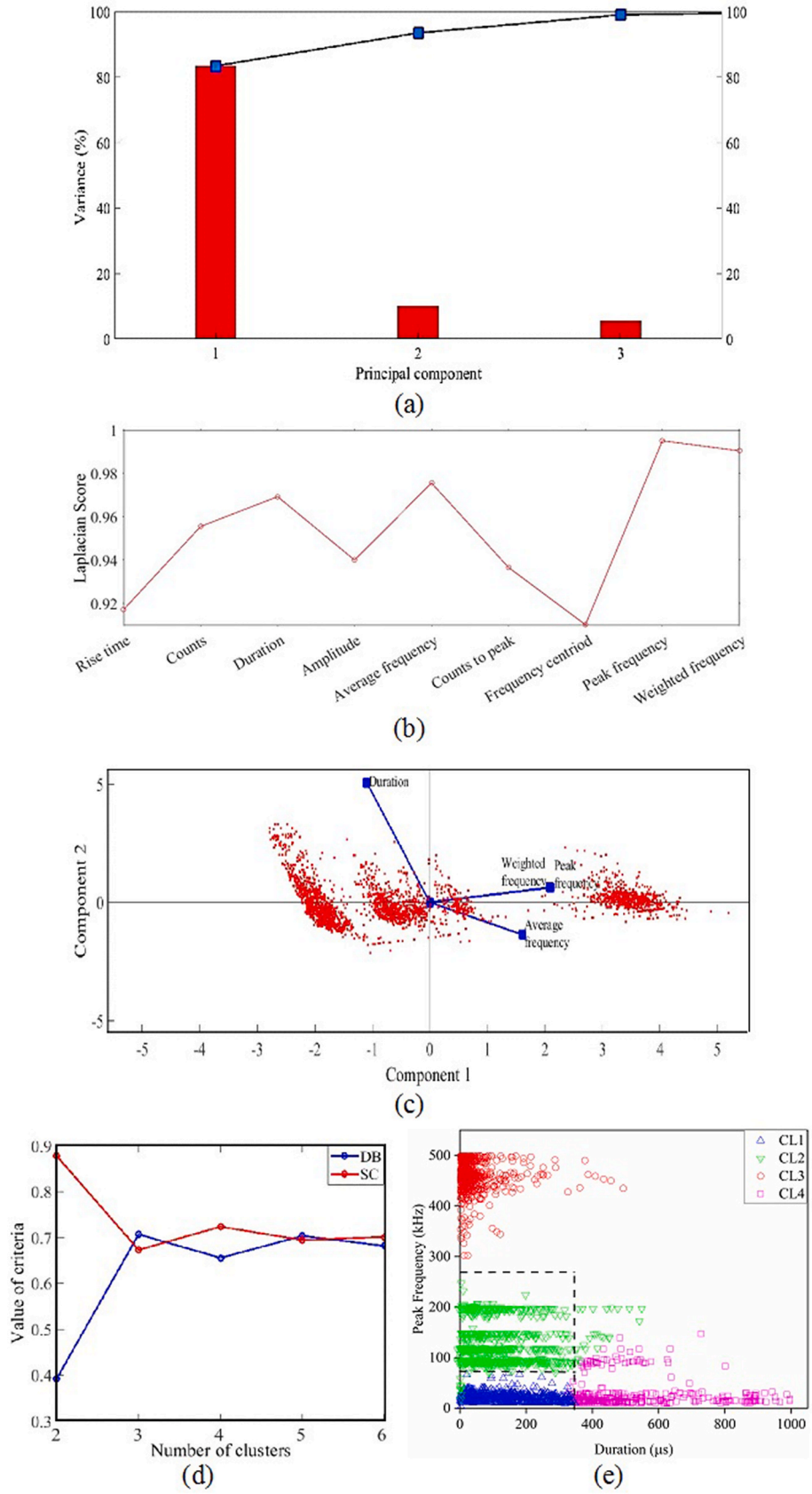

Fig. 5. a) Variance of principal components and their cumulative amounts. b) Laplacian score of various AE descriptors. c) Distribution of AE data in principal component subspace and score of AE parameters with highest Laplacian score. d) Values of Davies-Bouldin (DB) and Silhouette criteria (SC). e) Distribution of clusters for sample 1.

optimal cluster number. The clusters are best represented based on Peak Frequency (kHz) and Duration (μs) parameters graph. Fig. 5e shows the distribution of collected AE hits for Sp.1 during non-interrupted test with respect to the aforementioned two features. Clustering with k-means++ algorithm indicates the presence of 4 different classes of AE hits based on their similarities where each single AE hit recorded during the test is attributed to a specific group. According to a recent review by Barile et al. (2020) using Peak Frequency (kHz) besides relatively less utilized AE descriptors such as Duration (μs) can provide more reliable results. Moreover, the principal component analysis indicates that these two AE features have the least correlation among the other selected AE parameters. Accordingly, the k-means++ clustering of the registered AE events shows that the clusters are best represented with these parameters. The classification of clusters are shown in Table 1. The first cluster shown as CL1 is related to AE events with peak frequency between 0 and 70 kHz and duration between 0 and 350 μs. The AE hits with peak frequency between 70 and 250 kHz and duration between 0 and 550 μs are categorized in the second cluster, i.e. CL2. The AE hits which possess the highest peak frequency between 300 and 500 kHz and have duration in between 0 μs and 500 μs are registered as CL3. Finally, the AE hits classified as fourth cluster have peak frequency between 0 and 120 kHz and duration between 350 and 1000 μs. The apparent boundaries of clusters in two-dimensional space i.e. Peak Frequency vs Duration are given as dashed line in Fig. 5 for clarity.

Fig. 6a presents the load-displacement curve resulted from non-interrupted test combined with clustered AE hits recorded during loading. The initial elastic region of the test does not show any registered AE events which is consistent with the observations of previous studies (Li and Ma, 2020; Shi et al., 2014), in which no visible deformation-induced damage was reported in SPCs at the beginning of the flexural loading. Thus, the collected AE data at the elastic response region indicates no major failure under flexural loading. At about 2.5 mm of extension, the initial AE hit corresponding to CL3 is recorded which is characterized with high peak frequency and low duration. Almost immediately after the first recorded AE hit, other events correlated with CL2 are registered which have smaller peak frequency and less duration. These new AE hits are few individual events, and it must be noted that initiation of few signals should not be considered as a major damage mode. AE hits related to CL1 occur just after CL2 at about 2.5 mm deflection. Finally, the AE hits with low peak frequency and high duration characteristics associated with CL4 appear at 4.5 mm deflection. As seen in Fig. 6b, the occurrence frequency of AE activities increases continuously up to global failure of the Sp.1, thereby indicating the release of energy due to damage accumulation inside the material. According to (Liu et al., 2019; Giglio et al., 2012), the damage accumulation after elastic region of 3-point bending test for sandwich panels are related to core crushing, facesheet/core debonding, facesheet fiber breakage and matrix cracking damage types. Moreover, a previous study by authors (Tabrizi et al., 2019) has revealed that the loss of stiffness in laminated composites under flexural loading condition is correlated with simultaneous occurrence of different damage types, and initial AE cumulative energy release marks the start point of nonlinear behavior in material due to stiffness reduction. As seen in Fig. 6a, the linear region at the beginning of the test for Sp.1 can be represented by fitting a dashed line. Moreover, the initial AE hit observed at about 590 N is well correlated with the deviation point of load-displacement curve from the dashed fit line for linear elastic region. However, it must be noted that the occurrence of single or handful of AE incidents cannot cause stiffness reduction, whereas simultaneous and dense accumulation can be considered as initiation and progression of a damage mode that can result in major change of material behavior. The AE hit fraction associated with each cluster is given in Table 2, where the maximum failure types associated with 4th cluster and 1st cluster shows the lowest hit fraction.

Table 1
Classification of clusters.

		Peak Frequency (kHz)	Duration (μs)
△	CL1	$0 < \ldots < 70$	$0 < \ldots < 350$
▽	CL2	$70 \leq \ldots < 250$	$0 < \ldots < 550$
○	CL3	$300 < \ldots < 500$	$0 < \ldots < 500$
□	CL4	$0 < \ldots < 120$	$350 \leq \ldots < 1000$

The failure progress of Sp.1 as per Fig. 6 indicates that the initial failure is related to high peak frequency AE events. These types of events are generally referred to as fiber breakages in literature. However, it does not seem reasonable in this condition, since the failure of resin, facesheet/core interface and core can be expected earlier than load carrying fibers of the facesheet prepregs due to their lower strength. Using cumulative AE energy plot of Fig. 6c to monitor damage accumulation inside the sandwich laminate, one can see that energy release for various clusters increases continuously up to final failure point. The enclosed region by a dashed line in Fig. 6c marks the abrupt energy release associated with cluster 4 at maximum stress level. These high energy activities can be related to failure of the most recent load bearing constituent in the composite, reinforcing fibers. So it can be concluded that cluster 4 in this study is correlated with fiber damage in facesheets. Thermographs of the final failure of the sandwich panel after the non-interrupted test can be seen in Fig. 7 where the middle of core cells are distinguishable from cell walls. Various modes of thermography images are given to provide a better illustration of the failure region in sandwich panel. As seen in phasegram of Fig. 7a, in the middle of the sample, a transverse region with low phase is observed. This region indicates the final failure location of the sample directly under loading tip of the test apparatus. Such a vivid failure region is consistent with the significant energy release of cluster 4 as seen in Fig. 6c. Further analysis via amplitude full field maps in Fig. 7b reveals presence of two regions at the edge of the sample which are marked using dashed ovals. These two locations appear due to Poisson's effect in honeycomb core material under flexural loading condition and show severe deformation of core material. Moreover, Fig. 7b shows higher amplitude values (yellow color in color legend) in the middle portion of the broken sample as compared to upper and lower parts, thereby providing a relative assessment about the overall size of the failed region in the core material. As shown by black arrows in Fig. 7c, two high intensity locations along the transverse crack on facesheet are seen. These signified locations indicate crush of Nomex core honeycomb due to compressive stresses and buckling of cell walls. Fig. 7d gives a clear image of the crack propagated in transverse direction in fiber reinforced facesheet laminates. According to (Medina et al., 2020), transverse crack of the facesheet occurs at maximum flexural load level in sandwich panels and indicates failure threshold of the laminated structure. Image of the edge of Sp.1 through the thickness direction is presented in Fig. 7e, wherein the permanent crush in core cells is enclosed by dashed red line. On the other hand, micrograph seen in Fig. 7f shows the facesheet crack on the surface of sample reveals fiber failures and interlaminar delamination on the face sheets. Although several failure modes are indicated for uninterrupted test in thermography results, the correlation of acoustic emission results with each failure mode requires detailed investigation with interrupted test approach as follows.

The force-displacement curve for the first interrupted test is shown in Fig. 8a, where the initial elastic response of the sandwich panel is determined using a dashed fitting line. The initial registered AE activity related with CL4 cluster is linked to the deviation point of material behavior from linear behavior as shown with an arrow in Fig. 8. Immediate occurrence of AE hits related to clusters CL3 and CL1 after the first AE hit indicates the creation of damage involving multiple failure modes which reduce the stiffness of the sandwich material, being inferred from the apparent slope of load-deflection curve. Further loading of the sample is accompanied by damage accumulation and loss of stiffness up to the test stop point. As seen in Table 2, the relative fraction of AE hits for CL1, CL2, CL3 and CL4 at the interruption point of

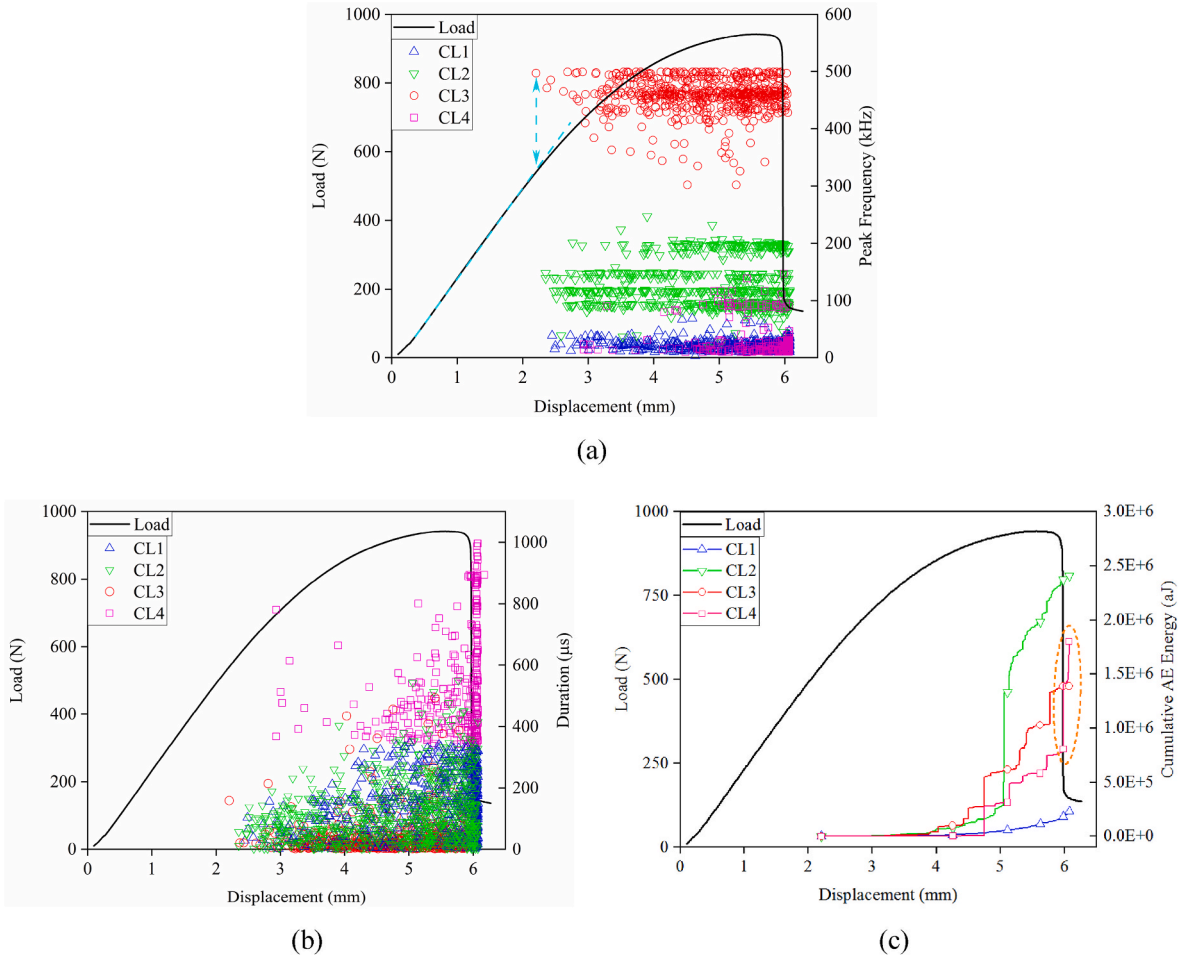

Fig. 6. a) Load - Peak Frequency vs. Displacement, b) Load - Duration vs. Displacement, c) Load - Displacement vs. Cumulative AE energy curves of the non-interrupted 3-point-bending test.

Table 2
AE hits fraction recorded during the tests.

		1st interrupted test	2nd interrupted test	Uninterrupted test
△	CL1	13	13	13
▽	CL2	20	40	26
○	CL3	62	39	28
□	CL4	5	8	33

the test are 13%, 20%, 62% and 6%, respectively. Although the dominant damage mode up to stop point of the first interrupted test is related to CL3, its prevalence is reduced to 28% for uninterrupted test as shown in Table 2. Moreover, the AE energy plot presented in Fig. 8b shows that the damage accumulation associated with CL3 releases the highest amount of energy at test stop point. So far, the final failure of the sample has not occurred, and it can be concluded that major AE energy release of CL3 seen in Fig. 8b is related to less stiff component of the sandwich laminates, i.e., core material. Moreover, in previous studies (Li and Ma, 2020; Zaharia et al., 2017; Liu et al., 2019), the initial major failures in sandwich structures are related to crushing of the soft-core material, and this type of failure gradually diminishes as the core material loses its out of plane strength and consequently stacking between the facesheets occurs. Hence, the AE hits observed in CL3 are correlated with core material failure as they appear in abundance at the beginning of the flexural tests and their relative fraction declines as the test proceeds. As seen in Table 2, the AE hits correlated with CL4 show the minimum fraction of damage types in the 1st interrupted test, while they appear as dominant failure events in the uninterrupted test. Such an abrupt increase in low frequency AE hits of CL4 from 6% to 33% can be interconnected with failures at skin components. According to experimental observations of authors in (Oz et al., 2017), low frequency AE hits can be related to fiber breakage in laminated composite materials. Since complete failure of sandwich facesheets, i.e. fiber breakage, is only observed in thermography images of Fig. 7 associated with uninterrupted test, one can conclude that the AE hits with low frequency related to CL4 are assigned to fiber failure events.

So far, the dominant failure mode in 1st interrupted test has been related to CL3 which is correlated to Nomex core failure. As seen in phasegram of Fig. 9a, there is a significant reduction of the width of core material due to Poisson's effect, and the thermography in Fig. 9b indicates that honeycomb cells in the middle of sample are not as vivid as the ones at upper and lower parts. These thermography images confirm that the significant AE hits of CL3 are correlated with deformation in honeycomb core and loss of out of plane strength for the sandwich composite at early stages occurs due to deformation of the core material rather than skin failure. To confirm this statement, the sample is cut from the middle in longitudinal direction for microscopic analysis. As indicated by enclosed red dashed lines in Fig. 9c the core material has permanently deformed due to applied flexural load. Although failure is permanent, it has not remained and it must be noted that other minor number of events registered during the test (Carvelli et al., 2017) indicate initiation of other damage modes in the sandwich structure namely, fiber breakage, matric cracking and facesheet/core debonding.

The load-displacement curve for 2nd interrupted test is given in

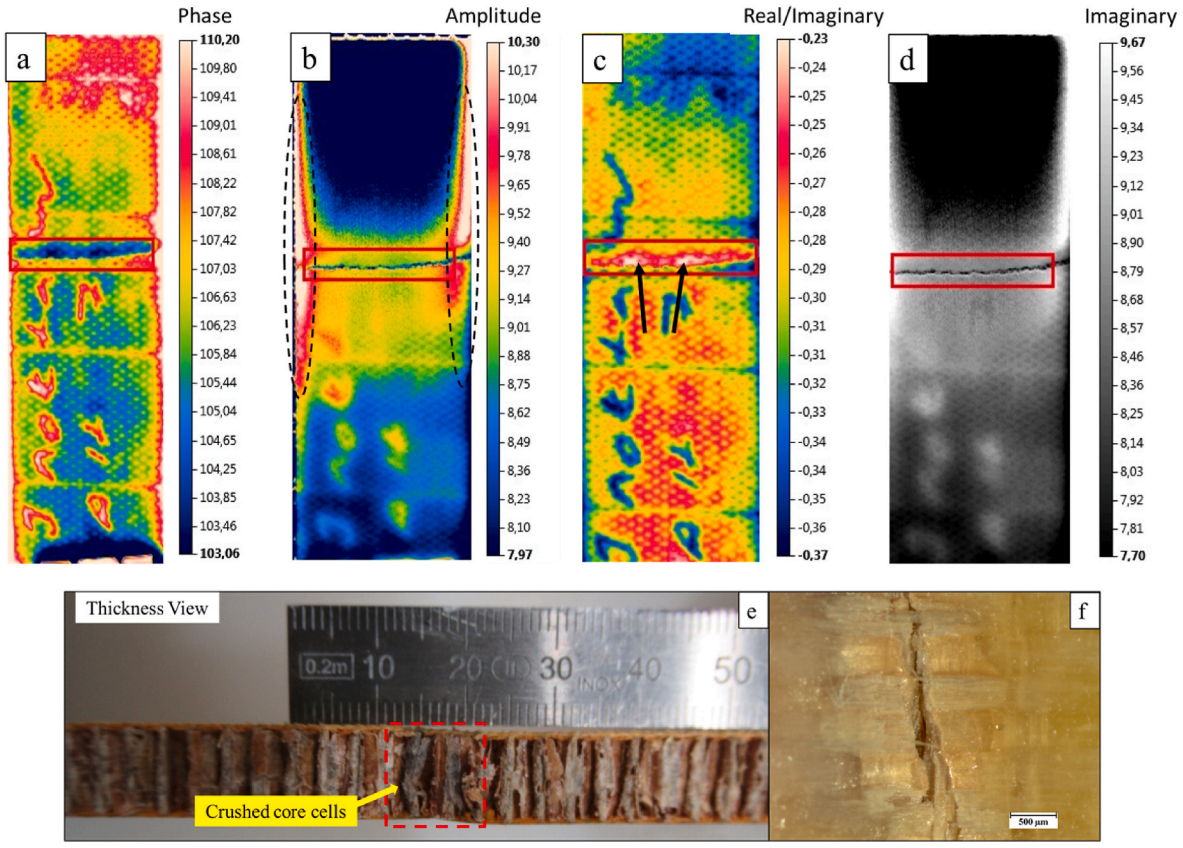

Fig. 7. (a–d) Thermograph of final failure of specimen 1 after non-interrupted test; (e) image of the failure area on the edge; (f) micrograph of the failure crack on face sheet.

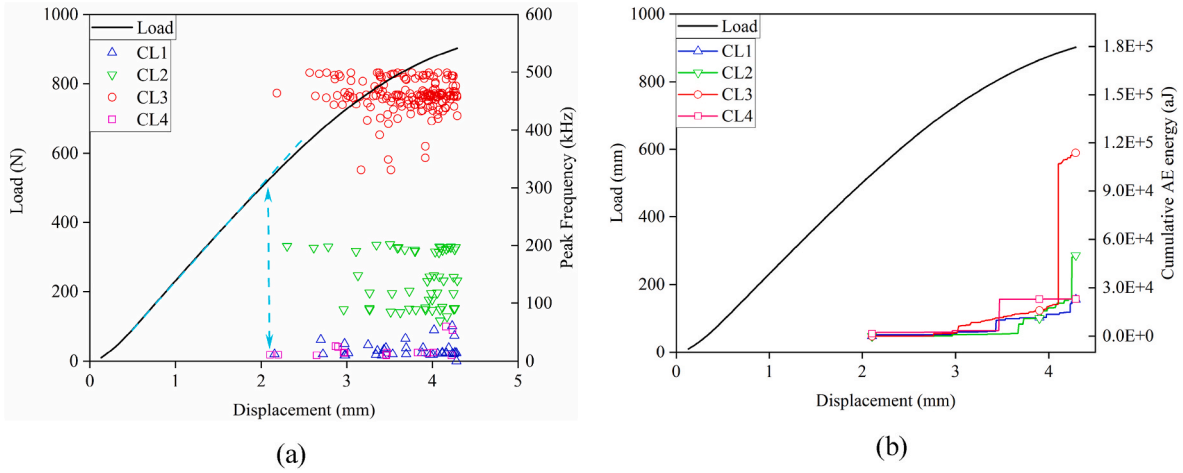

Fig. 8. a) Load - Peak Frequency vs. Displacement, b) Load - Displacement vs. Cumulative AE energy curves of 1st interrupted test.

Fig. 10a. Like previous cases, the deviation from initial linear behavior and start of the gradual loss of stiffness is corresponding to the first registered AE hit associated with CL3. The end point for the test is higher as compared to 1st interrupted test, therefore further development of damages inside the sandwich structure is expected. As seen in Fig. 10b, the highest AE energy release is related to CL3 which is followed by CL2. Since CL3 is corresponding to crush of the core material, therefore AE hits of CL2 will represent proximate damage mode to the failure of the core. The abrupt increase of AE energy for CL2 at test stop point shows that the relevant failure develops just after the crush of the core material associated with CL3. Accordingly, the relative fraction of AE hits related to CL1, CL2, CL3 and CL4 are 13%, 40%, 39% and 8%. The variation of AE hit fraction related to CL2 from 1st interrupted up to uninterrupted test in Table 2 implies that the relevant failure mode reaches to its maximum in 2nd interrupted test. To determine the failure mode(s) related to CL2, processed images of lock in thermography conducted after mechanical loading are given in Fig. 11. A significant anomaly in the middle of the sandwich panel is observed in phasegrams of Fig. 11a and b, which implies severe debonding between the top facesheet and the honeycomb core. Fig. 11c shows the micrograph of the middle of sample in thickness direction, where debonding (region enclosed in red dashed lines) between the facesheet and core cells is observed. While

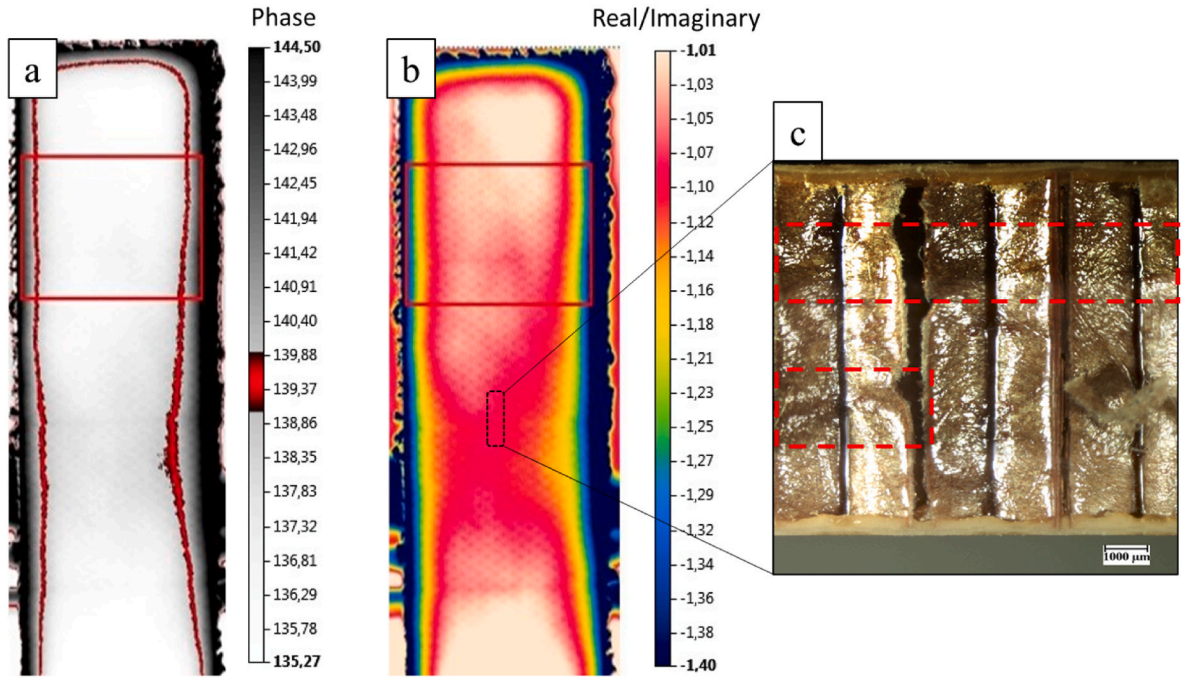

Fig. 9. (a–b) Thermographs of specimen at the end of 1st interrupted test (Sp.2 in Fig. 2); (c) micrograph of the thickness direction in the middle of sample.

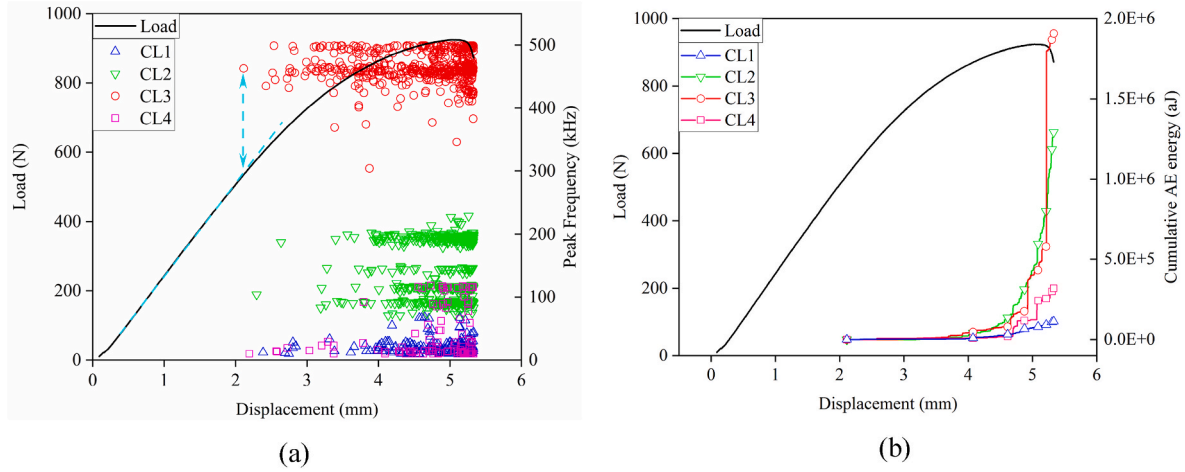

Fig. 10. a) Load - Peak Frequency vs. Displacement, b) Load - Duration vs. Cumulative AE energy curves of 2nd interrupted test.

debonding is seen at one side of the specimen, the opposite side does not reveal any debonding failure. Hence, it is confirmed that failure between facesheet and core cells occurs only at one side of the sample. Thus, sudden increase in AE hits related to CL2 can be correlated with debonding of facesheets from core material. The relative fraction of AE hits correlated with CL3 and CL2 in interrupted tests are also consistent with acceptable failure sequences provided in ASTM C393 standard (International, 2020), wherein initial failure modes under 3-point bending configuration must to be shear driven core failure and core/facesheet debonding. As shown in Fig. 11c, no significant failure in facesheets is observed after growth of debonding between the core material and facesheets. In contrast to the previous investigations, the fraction of AE hits for CL4 attributed to fiber breakage of facesheets does not show any significant increase even though the test is stopped after maximum loading point. This observation implies that debonding of core material from facesheets intensifies the loss of out of plane strength for SPCs, and load drop is not necessarily due to the skin material failure.

Fig. 12 shows that CL1 and CL2 have similar duration characteristics as registered during 2nd interrupted test. Besides, their initiation sequences are very close to each other. It means that these two clusters represent related damage modes. After initiation and growth of the delamination between facesheet and core, composite laminate of the skin provides the main resistance against the applied flexural load. In other words, the out of plane stiffness of the sandwich material is dependent on the strength of facesheets. According to previous studies, AE hits with low duration (Oz et al., 2019), and low frequency (Muhammad Awais Khan et al., 2021) are related to matrix microcracking. Therefore, the AE hits associated with CL1 are attributed to matrix failure in facesheets. It must be noted that the overall fraction of AE hits related to CL1 does not change for interrupted and uninterrupted tests, therefore indicating steady effect of matrix of facesheet in flexural behavior. Table 3 presents the overall sequence of damage progress under flexural loading condition for tested sandwich panels. According to registered AE hits and their fraction, it can be concluded that major damage initiates as core failure followed by debonding of facesheet/core. When the load carrying capacity of the core is diminished

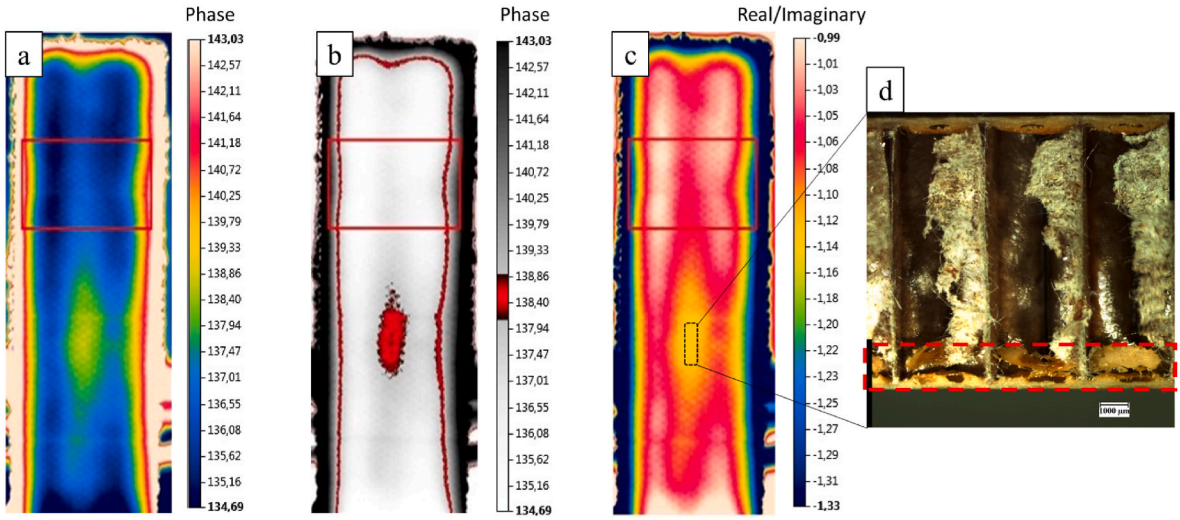

Fig. 11. (a–c) Thermographs of specimen at the end of 2nd interrupted test (Sp.3 in Fig. 2); (d) micrograph of the thickness direction in the middle of sample.

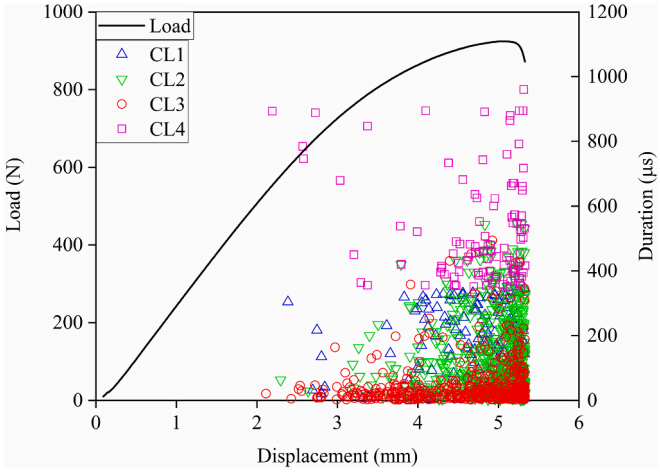

Fig. 12. Load - Duration vs. Displacement curve of 2nd interrupted test.

Table 3
Classification of AE hits according to damage modes.

Failure sequence			Peak Frequency (kHz)	Duration (µs)	Damage Modes
1	○	CL3	300 < … < 500	0 < … < 500	Core failure
2	▽	CL2	70 ≤ … < 250	0 < … < 550	Facesheet/core debonding
3	△	CL1	0 < … < 70	0 < … < 350	Matrix microcracks
4	□	CL4	0 < … < 120	350 ≤ … < 1000	Fibre breaks in facesheets

due to debonding and stacking of sandwich layers, the facesheets start to withstand to the applied load. Finally, failure of the facesheets due to matrix cracking and fiber breakage with low peak frequency values occurs almost concurrently sequence.

4. Conclusion

Single layer glass fiber reinforced phenolic skinned Nomex® honeycomb core composite sandwich panels not only provide high flexural rigidity and stiffness but also deliver flame retardancy which makes them suitable for interior components of aircraft. The major advantage of the proposed methodology is assessment of internal failure progress based on thermography images obtained after interrupted tests rather than visual inspection from side of the sample which is typically conducted in other investigations. Moreover, the evaluation and clustering of acoustic emission data to identify major damage sequence in sandwich structures is achieved via correlation of thermography results with change of fraction of AE clusters. The results of this investigation provide a comprehensive insight about various stages of failure development under flexural loading condition in sandwich composites. This approach is shown to yield promising results in terms of identification of damage modes during loading. k-means++ algorithm was implemented to determine four clusters of acoustic emission hits relying on their duration and peak frequency. Based on percentage of each cluster during the interrupted and uninterrupted tests, and the observation of major damages appearing in the thermography results after each test, following sequence of failure is determined for sandwich panels under flexural loading condition. It is concluded that the core failures in honeycomb are detected with high frequency clusters as initial major damage type. Then, the mid frequency acoustic emission cluster, which is seen as delaminations between the facesheets and the core in thermography results occurs. The next major failure is correlated with matrix cracks in the facesheets, which preserves a constant fraction of all acoustic emission hits. Finally, the fibre breakages with low frequency and highest duration values mark the final failure of sandwich panel as they only appear in thermography results of the uninterrupted test. Comparison of postmortem thermography phasegram of interrupted test with load-displacement curve showed that sandwich panel samples could have exceeded the maximum load level without any major transverse cracks in the facesheets. Therefore, it is concluded that the main drop of out of plane strength could also be a result of debonding between facesheets and core material. The novel approach based on the interrupted tests along with active thermography used in this study provide a solid methodology to determine the invisible failure stages and damage progress in flame retardant composite sandwich panels through utilizing structural health monitoring techniques.

Declaration of competing interest

The authors declare that they have no known competing financial interests or personal relationships that could have appeared to influence the work reported in this paper.

Acknowledgement

Authors acknowledge Kordsa for providing materials. We also acknowledge Prof. S.V. Lomov from Materials Engineering Department of KU Leuven for providing access to k-means++ clustering algorithm.

References

Akay, E., et al., 2016. Monitoring Poisson's ratio degradation of FRP composites under fatigue loading using biaxially embedded FBG sensors. Materials 9 (9), 781.
AlKhateab, B., et al., 2020. Damage mechanisms in CFRP/HNT laminates under flexural and in-plane shear loadings using experimental and numerical methods. Compos. Appl. Sci. Manuf. 136, 105962.
Anandan, S., et al., 2020. Investigation of sandwich composite failure under three-point bending: simulation and experimental validation. J. Sandw. Struct. Mater. 22 (6), 1838–1858.
Barile, C., et al., 2020. Application of different acoustic emission descriptors in damage assessment of fiber reinforced plastics: a comprehensive review. Eng. Fract. Mech. 235, 107083.
Ben Ammar, I., et al., 2014. Mechanical behavior and acoustic emission technique for detecting damage in sandwich structures. Appl. Acoust. 86, 106–117.
Beylergil, B., et al., 2020a. Experimental failure analysis and mechanical performance evaluation of fiber-metal sandwich laminates interleaved with polyamide-6,6 (PA 66) interlayers through the combined usage of acoustic emission, thermography and microscopy techniques. J. Sandw. Struct. Mater. 0(0).
Beylergil, B., et al., 2020b. Experimental failure analysis and mechanical performance evaluation of fiber-metal sandwich laminates interleaved with polyamide-6,6 interlayers through the combined usage of acoustic emission, thermography and microscopy techniques. J. Sandw. Struct. Mater. 0(0): p. 1099636220924654.
Carvelli, V., D'Ettorre, A., Lomov, S.V., 2017. Acoustic emission and damage mode correlation in textile reinforced PPS composites. Compos. Struct. 163, 399–409.
Ciampa, F., Meo, M., 2010. A new algorithm for acoustic emission localization and flexural group velocity determination in anisotropic structures. Compos. Appl. Sci. Manuf. 41 (12), 1777–1786.
Dikshit, V., et al., 2021. Quasi-static indentation analysis on three-dimensional printed continuous-fiber sandwich composites. J. Sandw. Struct. Mater. 23 (2), 385–404.
Essassi, K., et al., 2020. Experimental and analytical investigation of the bending behaviour of 3D-printed bio-based sandwich structures composites with auxetic core under cyclic fatigue tests. Compos. Appl. Sci. Manuf. 131, 105775.
Giglio, M., Gilioli, A., Manes, A., 2012. Numerical investigation of a three point bending test on sandwich panels with aluminum skins and Nomex (TM) honeycomb core. Comput. Mater. Sci. 56, 69–78.
Harizi, W., et al., 2021. Mechanical behavior of carbon-reinforced thermoplastic sandwich composites with several core types during three-point bending tests. Compos. Struct. 262, 113590.
He, Y.Z., et al., 2021. An overview of acoustic emission inspection and monitoring technology in the key components of renewable energy systems. Mech. Syst. Signal Process. 148, 107146.
International, A., 2020. ASTM C393/C393M-20, Standard Test Method for Core Shear Properties of Sandwich Constructions by Beam Flexure.
Kefal, A., et al., 2021. An experimental implementation of inverse finite element method for real-time shape and strain sensing of composite and sandwich structures. Compos. Struct. 258, 113431.
Khan, R.M.A., et al., 2020. Investigation on interlaminar delamination tendency of multidirectional carbon fiber composites. Polym. Test. 90, 106653.
Kocaman, E.S., et al., 2017. Monitoring the damage state of fiber reinforced composites using an FBG network for failure prediction. Materials 10 (1), 32.
Lainé, E., et al., 2020. Acoustic emission description from a damage and failure scenario of rotomoulded polyolefin sandwich structure subjected to internal pressure for storage applications. Mech. Indust. 21 (1), 105.
Lee, K.-H., Gu, J.-U., Choi, N.-S., 2009. Acoustic emission characteristics and fracture behaviors of GFRP-aluminum honeycomb hybrid laminates under compressive and bending loads. Comp. Res. 22 (6), 23–31.
Leone, F., et al., 2008. Acoustic emission analysis of full-scale honeycomb sandwich composite curved fuselage panels. SPIE Smart Struct. Mater. Nondestr. Eval. Health Monitor. 6934 (SPIE).
Li, Z., Ma, J., 2020. Experimental study on mechanical properties of the sandwich composite structure reinforced by basalt fiber and Nomex honeycomb. Materials 13 (8), 1870.
Li, L., et al., 2014. Cluster analysis of acoustic emission signals for 2D and 3D woven glass/epoxy composites. Compos. Struct. 116, 286–299.
Li, L., Lomov, S.V., Yan, X., 2015. Correlation of acoustic emission with optically observed damage in a glass/epoxy woven laminate under tensile loading. Compos. Struct. 123, 45–53.
Liu, Y., et al., 2019. Mechanical responses of a composite sandwich structure with Nomex honeycomb core. J. Reinforc. Plast. Compos. 38 (13), 601–615.
Masmoudi, S., El Mahi, A., Turki, S., 2015. Use of piezoelectric as acoustic emission sensor for in situ monitoring of composite structures. Compos. B Eng. 80, 307–320.
Masoudi Moghaddam, S., et al., 2020. Mechanical behavior of sandwich panels with hybrid face sheets and embedded super-elastic SMA wires under quasi-static loading: an experimental investigation. Int. J. Damage Mech. 0(0): p. 1056789520953465.
McGugan, M., et al., 2006. Detecting and Identifying Damage in Sandwich Polymer Composite by Using Acoustic Emission.
Medina, S., Meza, J., Kawashita, L.F., 2020. Damage sequence of honeycomb sandwich panels under bending loading: experimental and numerical investigation. J. Reinforc. Plast. Compos. 39 (5–6), 175–192.
Meola, C., et al., 2006. Non-destructive evaluation of aerospace materials with lock-in thermography. Eng. Fail. Anal. 13 (3), 380–388.
Muhammad Awais Khan, R., et al., 2021. A novel hybrid damage monitoring approach to understand the correlation between size effect and failure behavior of twill CFRP laminates. Compos. Struct. 114064.
Olsson, R., 1998. Methodology for Predicting the Residual Strength of Impacted Sandwich Panels.
Oz, F.E., Ersoy, N., Lomov, S.V., 2017. Do high frequency acoustic emission events always represent fibre failure in CFRP laminates? Compos. Appl. Sci. Manuf. 103, 230–235.
Oz, F.E., et al., 2018. Multi-instrument in-situ damage monitoring in quasi-isotropic CFRP laminates under tension. Compos. Struct. 196, 163–180.
Oz, F.E., Ahmadvashaghbash, S., Ersoy, N., 2019. Damage mode identification in transverse crack tension specimens using acoustic emission and correlation with finite element progressive damage model. Compos. B Eng. 165, 84–95.
Oz, F.E., Calik, E., Ersoy, N., 2020. Finite element analysis and acoustic emission monitoring of progressive failure of corrugated core composite structures. Compos. Struct. 253, 112775.
Quispitupa, A., et al., 2004. Acoustic emission based tensile characteristics of sandwich composites. Compos. B Eng. 35 (6), 563–571.
Saeedifar, M., Zarouchas, D., 2020. Damage characterization of laminated composites using acoustic emission: a review. Compos. B Eng. 195, 108039.
Saeedifar, M., et al., 2021. Damage assessment of a titanium skin adhesively bonded to carbon fiber-reinforced plastic omega stringers using acoustic emission. Struct. Health Monit.
Selmi, S., et al., 2020. Characterisation of natural flax fibers honeycomb: compression damage analysis using acoustic emission. J. Nat. Fibers 1–10.
Seno, A.H., Khodaei, Z.S., Aliabadi, M.F., 2019. Passive sensing method for impact localisation in composite plates under simulated environmental and operational conditions. Mech. Syst. Signal Process. 129, 20–36.
Shi, S.-s., et al., 2014. Carbon-fiber and aluminum-honeycomb sandwich composites with and without Kevlar-fiber interfacial toughening. Compos. Appl. Sci. Manuf. 67, 102–110.
Shrestha, R., Choi, M., Kim, W., 2019. Thermographic inspection of water ingress in composite honeycomb sandwich structure: a quantitative comparison among Lock-in thermography algorithms. Quant. InfraRed Thermogr. J. 1–16.
Sikdar, S., Ostachowicz, W., Pal, J., 2018. Damage-induced acoustic emission source identification in an advanced sandwich composite structure. Compos. Struct. 202, 860–866.
Sikdar, S., et al., 2019. Damage-induced acoustic emission source monitoring in a honeycomb sandwich composite structure. Compos. B Eng. 158, 179–188.
Tabrizi, I.E., et al., 2019. Experimental and numerical investigation on fracture behavior of glass/carbon fiber hybrid composites using acoustic emission method and refined zigzag theory. Compos. Struct.
Tabrizi, I.E., et al., 2021. Using digital image correlation for in situ strain and damage monitoring in hybrid fiber laminates under in-plane shear loading. Polym. Compos. 42 (8), 4029–4042.
Taraghi, I., Fereidoon, A., 2016. Non-destructive evaluation of damage modes in nanocomposite foam-core sandwich panel subjected to low-velocity impact. Compos. B Eng. 103, 51–59.
Topkaya, T., Solmaz, M., 2016. Fatigue Behavior of Honeycomb Sandwich Composites under Flexural and Buckling Loading, pp. 177–182.
Toscano, C., et al., 2014. On the use of lock-in thermography to monitor delamination growth in composite panels under compression. Sci. Eng. Compos. Mater. 21 (4), 485–492.
Uzal, A., et al., 2018. A composite sandwich plate with a novel core design. Compos. Struct. 193, 198–211.
Wu, Y., et al., 2021. On the determination of acoustic emission wave propagation velocity in composite sandwich structures. Compos. Struct. 259, 113231.
Yilmaz, C., Yildiz, M., 2017. A study on correlating reduction in Poisson's ratio with transverse crack and delamination through acoustic emission signals. Polym. Test. 63, 47–53.
Yilmaz, C., et al., 2016. Monitoring Poisson's ratio of glass fiber reinforced composites as damage index using biaxial Fiber Bragg Grating sensors. Polym. Test. 53, 98–107.
Yilmaz, C., et al., 2020. Non-destructive determination of the stiffness matrix of a laminated composite structure with lamb wave. Compos. Struct. 237, 111956.
Zaharia, S., et al., 2017. Mechanical properties and fatigue performances on sandwich structures with CFRP skin and Nomex honeycomb core. Mater. Plast. 54, 67–72.
Zhao, H., et al., 2017. Application of lock-in thermography for the inspection of disbonds in titanium alloy honeycomb sandwich structure. Infrared Phys. Technol. 81, 69–78.